Natural Abundance ^{15}N and ^{13}C Solid-State NMR Chemical Shifts: High Sensitivity Probes of the Halogen Bond Strength

Paolo Cerreia Vioglio,[†] Luca Catalano,[‡] Vera Vasylyeva,[‡] Carlo Nervi,[†] Michele R. Chierotti,[†] Giuseppe Resnati,[‡] Roberto Gobetto*[†] and Pierangelo Metrangolo*[‡§]

[†]Department of Chemistry and NIS Center, University of Torino, via P. Giuria 7, 10125 Torino, Italy.

[‡]Laboratory of Nanostructured Fluorinated Materials (NFMLab), Department of Chemistry, Materials, and Chemical Engineering "Giulio Natta", Politecnico di Milano, via L. Mancinelli 7, 20131 Milano, Italy.

[§]VTT-Technical Research Centre of Finland, Biologinkuja 7, 02150 Espoo, Finland.

ABSTRACT: Solid-State Nuclear Magnetic Resonance (SSNMR) is a versatile characterization technique that can provide a plethora of information complementary to Single Crystal X-Ray Diffraction (SCXRD) analysis. However, the latter is still pivotal in assessing the halogen bond (XB) occurrence and having a rough estimation of its strength through the normalized distance parameter (R_{XB}), obtained from experimental crystallographic data. Herein, we present an experimental and computational investigation of the relationship between the strength of an XB and the SSNMR chemical shifts of the non-quadrupolar nuclei either directly involved in the interaction (^{15}N) or covalently bonded to the halogen atom (^{13}C). We have prepared two series of X-bonded co-crystals based upon two different dipyridyl modules, and several halobenzenes and diiodoalkanes, as XB-donors. SCXRD structures of three novel co-crystals between 1,2-bis(4-pyridyl)ethane, and 1,4-diiodobenzene, 1,6-diiodododecafluorohexane, and 1,8-diiodohexadecafluorooctane are reported. For the first time, the change in the ^{15}N SSNMR chemical shifts upon XB formation is shown to experimentally correlate with the strength of the XB. The same overall trend is confirmed by density functional theory (DFT) calculations of the chemical shifts. [13]C NQS experiments show a positive, linear correlation between the chemical shifts and the C–I elongation, which is an indirect probe of the strength of the XB. These correlations can be of general utility to estimate the strength of the XB occurring in diverse adducts by using affordable SSNMR analysis.

In recent years, halogen bonding (XB) has been attracting increasing attention thanks to its applications in different fields, *e.g.*, crystal engineering, materials chemistry, and biochemistry.[1-3] The success of this specific noncovalent interaction derives from its unique physico-chemical properties, namely strength, selectivity, tunability, and directionality.[4,5] XB spans an energy range similar to that of the more commonly used hydrogen bonding, *i.e.*, 5–200 kJ/mol.[6] By changing the XB-donor atom involved in the interaction or its covalently-bound substituents it is possible to fine-tune the final strength of the XB, an extremely useful feature for the design of new supramolecular species.[7] In addition, XB is strongly directional,[8,9] thus enabling the predictable alignment of molecular building blocks into crystalline architectures and functional materials, such as photoresponsive polymers, pharmaceutical co-crystals, porous materials, among others.[10-14] XB plays also a key role in anion recognition and coordination both in solid state and in solution,[15,16] ability of relevant interest especially for biological systems.[17]

The 2013 IUPAC XB definition states: "A halogen bond occurs when there is evidence of a net attractive interaction between an electrophilic region associated with a halogen atom in a molecular entity and a nucleophilic region in another, or the same, molecular entity".[18] The counterintuitive electrophilic behavior of the elements of the XVII group arises from the anisotropic molecular electrostatic potential distribution around halogens atoms, which shows the emergence of a region of positive electrostatic potential, called σ-hole, along the extension of the covalent bond the halogen atom is involved in.[19]

The XB occurrence can be detected by a number of analytical techniques: since the first studies in the 1960's, the most employed ones are single crystal X-ray diffraction (SCXRD) analysis, nuclear magnetic resonance (NMR), vibrational and UV-visible spectroscopies, and thermal analysis.[20] However, XB has long been studied in the solid state mainly by X-ray diffraction techniques,[1] while NMR spectroscopy has been traditionally adopted only to shed light on its solution behavior.[21] IR and Raman spectroscopies have been applied both in solution and in the solid state.[22] These studies in condensed phases have been corroborated by gas phase investigations,[23] as well as data mining from crystallographic databases such as the CSD.[1,8,24] Moreover, computational studies have been crucial to elucidate the nature of XB or to fully understand the structural changes observed upon XB formation.[25,26] Within this framework,

NMR techniques offer unique opportunities to the study of XB. Solution NMR spectroscopy has proven to be a convenient and sensitive tool to establish the occurrence of XB in supramolecular adducts, to rank the ability of XB donors and acceptors, and even to describe thermodynamic and geometric characteristics of formed adducts.[5,12,27-33]

Unlike solution NMR, detailed studies of XB by solid-state NMR (SSNMR) have been carried out only in recent years, although some ^{13}C CPMAS data of a complex between 1,4-diazabicyclo[2.2.2]octane and CBr_4 were already reported by Kochi in 1987.[34] Recently, efforts are directed to in-depth, specialized SSNMR analysis, with multinuclear approaches and systematic resort to quantum chemical calculations with DFT-based methods.

XB can be probed by looking at the atoms close to the interaction: the halogen atom, the carbon covalently bonded to it, and the nitrogen (if present). While the acquisition/interpretation of both ^{13}C and ^{15}N spectra is straightforward since it is based on the variation of the chemical shift parameter upon XB formation, the acquisition/interpretation of halogen atoms spectra is still challenging. Indeed, [35/37]Cl, [79/81]Br, and [127]I are all quadrupolar nuclei (i.e., I > ½) with very high quadrupolar coupling constants. This leads to very broad lines (in the order of tens of MHz) that require a combination of sophisticated hardware and techniques to be employed, such as very high magnetic fields (up to 21 T), ultra-fast MAS (up to 100 kHz), acquisition of several subspectra to be added for collecting the whole signal, and special pulse sequences (QCPMG). On the other hand, quadrupolar nuclei provide several other interesting parameters in addition to the chemical shift, such as quadrupolar coupling constants and electric field gradient tensors that add further insights into the halogen environment, and thus into the XB. Bouchmella et al. have demonstrated that SSNMR is a sensitive technique to detect XB formation: they have studied X-bonded imidazole and morpholine-based compounds, which show an increase of the ^{15}N chemical shifts as the intermolecular N⋯I distance increases.[35] Shortly after, Weingarth et al. have determined the intermolecular N⋯I distance by studying the dipolar ^{15}N/[127]I coupling in a ^{15}N-enriched benzyl-di(4-iodobenzyl)amine.[36] Viger-Gravel et al. have published a detailed study on thiocyanate anions X-bonded to diiodo-perfluoroarenes.[37] [13]C chemical shifts were found to increase in the presence of XB compared to reference unbonded compounds, while ^{15}N chemical shifts were found to decrease under the same conditions. Selenocyanates were noted to show the opposite trends. Bryce and coworkers have used high-field SSNMR to directly probe weak XBs involving [35]Cl, [81]Br, and [127]I in various solid haloanilinium halides,[38] where the authors found interesting correlations between isostructural compounds. Widdifield et al. have, instead, reported a multinuclear study on a series of decamethonium diiodide-dihalogenated benzene co-crystals.[39] They have carried out ^{13}C, [14/15]N, ^{19}F, and [127]I SSNMR experiments to examine the effect of XB occurrence on several NMR parameters. In particular, XB was found to cause ^{13}C chemical shift increase at the carbon atom directly adjacent to the XB-donor, as well as the [14]N

and [127]I quadrupolar coupling constants were judged sensitive probes of the co-crystals formation. Viger-Gravel et al. established a correlation between ^{13}C chemical shift values and C–I bond lengths in co-crystals of 1,4-diiodotetrafluorobenzene with ammonium or phosphonium halide salts.[40] Despite the discrepancies found between experimental and computed data, they were able to conclude that the chemical shift increases as the C–I distance increases. Recently, Bryce and co-workers have performed a multifaceted study on iodobenzene-onium halide co-crystals exhibiting C–I⋯X[-] interactions. They have confirmed that ^{13}C chemical shifts are diagnostic of the strength of the XB; at the same time they have found a correlation between quadrupolar NMR parameters and the local XB geometry.[41]

Few other SSNMR investigations on XB are also reported in the literature[42-44] and there is still a need for a multinuclear SSNMR investigations in order to find a systematic relationship between the changes in chemical shift of atoms involved in XB and the strength of the interaction. Indeed, clear and general relationships between NMR parameters and x-ray data are still missing. For this reason, we performed a complete screening by ^{15}N and ^{13}C SSNMR of different XB-donors in two series of X-bonded supramolecular structures, constructed by assembling dipyridyl derivatives and either halobenzenes or haloalkanes. The investigation of strength and structural organization has been carried out by a combined SSNMR, FTIR, SCXRD, and computational approach. Three new X-bonded adducts between 1,2-bis(4-pyridyl)ethane as XB acceptor and 1,4-diiodobenzene, 1,8-diiodohexadecafluorooctane, and 1,6-diiodododecafluorohexane are also reported.
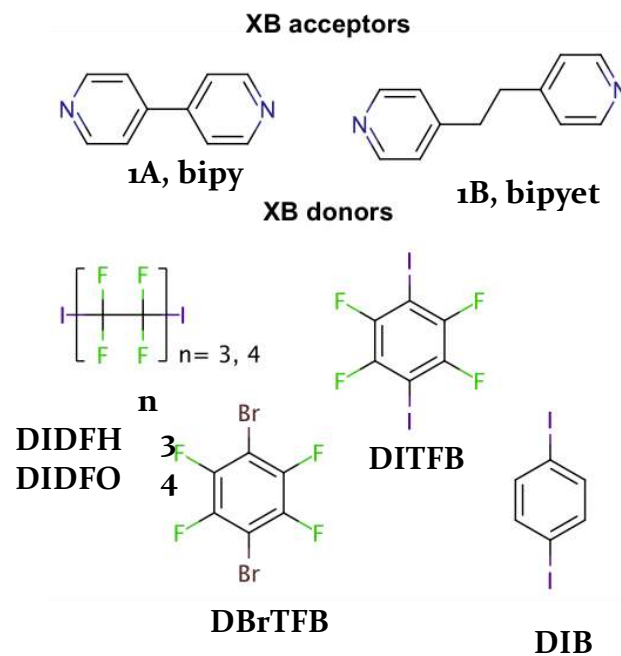
Figure 1. Molecular building blocks of the X-bonded co-crystals under study.

EXPERIMENTAL SECTION

Supramolecular synthesis. All the starting materials were purchased from Sigma-Aldrich and were used without further purification. At room temperature, equimolar amount of 4,4'-bipyridine (**1A**, bipy) or 1,2-bis(4-pyridyl)ethane (**1B**, bipyet) were dissolved in acetone with 1,8-diiodohexadecafluorooctane (DIHFO), 1,6-diiodododecafluorohexane (DIDFH) or 1,4-diiodotetrafluorobenzene (DITFB). At room temperature, equimolar amounts of either **1A** or **1B** were also dissolved in chloroform with 1,4-dibromotetrafluorobenzene (DBrTFB) and in dichloromethane with 1,4-diiodobenzene (DIB). All the solutions were put in vials and then placed in jars containing paraffin oil and sealed. All of the adducts were obtained in the form of good-quality single crystals by slow-evaporation of the solvent. The crystalline products were all washed with cold heptane before further characterization. The obtained adducts are shown in Table 1.

Table 1. Obtained halogen-bonded co-crystals.

	Co-cryst
[(**1A**)·(1,4-dibromotetrafluorobenzene)]	**2A**
[(**1A**)·(1,4-diodobenzene)]	**3A**
[(**1A**)·(1,4-diiodotetrafluorobenzene)]	**4A**
[(**1A**)·(1,8-diiodohexadecafluorooctane)]	**5A**
[(**1A**)·(1,6-diiodododecafluorohexane)]	**6A**
[(**1B**)·(1,4-dibromotetrafluorobenzene)]	**2B**
[(**1B**)·(1,4-diodobenzene)]	**3B**
[(**1B**)·(1,4-diiodotetrafluorobenzene)]	**4B**
[(**1B**)·(1,8-diiodohexadecafluorooctane)]	**5B**
[(**1B**)·(1,6-diiodododecafluorohexane)]	**6B**

Thermal analysis. DSC analyses were performed using a Mettler Toledo DSC 823e. 2–20 mg of each sample were closed in an aluminum pan and measured with heating/cooling rates of 10 °C/min.

Single crystal X-ray diffraction analysis. The crystals were measured using Mo-Kα radiation on a Bruker KAPPA APEX II diffractometer with a Bruker KRYOFLEX low temperature device. Formation of co-crystals **2A**, **3A**, **4A**, **5A**, **6A**, **2B**, **4B**, **5B**, and **6B** was confirmed by crystal cell determination and comparison with previously reported data.[4,28,45] Crystal structures of the new adducts **3B**, **5B**, and **6B** were solved by direct method and refined against F² using SHELXL97.[46] Packing diagrams were generated using Mercury.[47] Intermolecular interactions were analyzed with PLATON.[48] The non-hydrogen atoms were refined anisotropically and hydrogen atoms were refined using difference Fourier map or positioned geometrically. **Selected crystallographic data and** supramolecular infinite chain within the crystal structure **for co-crystals 3B, 5B and 6B are reported in SI.**

Powder X-ray diffraction analysis. A Bruker AXS D8 powder diffractometer was used for all PXRD measurements with experimental parameters as follows: Cu-Kα radiation. Scanning interval: 5–40° 2θ. The experimental PXRD patterns and calculated PXRD patterns from single crystal structures were compared to confirm the composition of bulk materials.

IR-spectroscopy. IR spectra were obtained using a Nicolet iS50 FTIR spectrometer equipment with ATR device. For each compound two different spectra were collected: Far IR spectrum (128 scans, 100–1000 cm⁻¹) using solid substrate beam splitter; middle IR (32 scans, 1000–4000 cm⁻¹) with KBr beam splitter. All the spectra were measured with a resolution of ±4 cm⁻¹ and corrected with the baseline correction tool of the OMNIC software.

Computational details. Periodic lattice calculations were performed by means of Quantum Espresso version 5.1.2.[49] The Generalized Gradient Approximation (GGA) functional PW86PBE,[50,51] with the inclusion of the exchange-hole dipole moment (XDM)[52] dispersion correction method for accurate model of the X-bonded interactions was used in all calculations. XDM dispersion energies were computed using the modified version of Quantum Espresso, adopting the appropriate damping parameters for the functional PW86PBE (a1 = 0.6836 and a2 = 1.5045).[52a] For geometry optimizations, the solid-state crystal structures from either the literature or the present study (*i.e.*, **3B**, **5B**, and **6B**) were considered as starting structures. Calculations were performed with the variable-cell scheme, adopting the Kresse-Joubert Projected Augmented Wave pseudopotentials.[53] A cut-off of 60 Ry was used for structural optimization. The NMR chemical shifts were calculated using an 80 Ry energy cut-off by the GIPAW method.[54] A 60 Ry cut-off for NMR calculations gave unsatisfactory results, but values higher than 80 Ry did not significantly improved the quality of the data. The theoretical absolute magnetic shielding (σ) values were converted into chemical shift scale (δ) by subtracting the shielding values from the experimental absolute shielding value of liquid ammonia at 300 K, 244.6 ppm, given in literature.[55] Additional chemical shift calculation details may be found in the Supporting Information (SI), Table S1. The Brillouin zones were automatically sampled with the Monkhorst-Pack scheme,[56] in a similar approach as previously described.[57] Geometry optimization, phonon and NMR chemical shift calculations for compounds **2A**, **3A**, **4A**, **5A**, **6A**, **2B**, **3B**, **4B**, **5B**, **6B** were performed with a grid mesh of 2×1×1, 2×2×2, 2×2×1, 3×2×1, 2×1×2, 1×2×1, 3×1×1, 3×1×1, and 3×1×1, respectively. For compounds **1A**, and **1B** grid meshes of 2×2×1 and 3×1×2 were respectively used.

Solid-State NMR Spectroscopy. SSNMR measurements were carried out on a Bruker AVANCE II 400 instrument operating at 400.23, 376.55, 100.65 and 40.56 MHz for ¹H, ¹⁹F, ¹³C and ¹⁵N, respectively. Powdered samples were packed in cylindrical 4 mm o.d. zirconia rotors, with sample volume of 80 μL.

¹⁵N CPMAS (cross-polarization magic-angle spinning) spectra were recorded at room temperature at the spinning speed of 9 kHz. A ramp cross-polarization pulse sequence[58]

was used with contact time of 4 ms, a ¹H 90° pulse of 3.80 µs, recycle delays ranging from 5 to 60 s, and 2048–10240 transients. The two pulse phase modulation (TPPM) decoupling scheme[59] was used with a frequency field of 66 kHz. All spectra were acquired with a resolution of 0.5 ppm.

¹³C non-quaternary suppression (NQS) spectra were collected at room temperature at spinning speed of 12 or 13 kHz, with ¹³C 180° refocusing pulse of 9.20 µs and dephasing times ranging from 40 to 55 µs. The pulse width and the RF power were finely adjusted for best resolution. ¹H/¹³C ramp cross-polarization pulse sequence was used with contact time of 9 ms, a ¹H 90° pulse of 4.00 µs, recycle delays ranging from 5 to 60 s, and 1440–7680 transients. ¹⁹F/¹³C ramp cross-polarization pulse sequence was employed with contact time of 9 ms, a ¹⁹F 90° pulse of 3.40 µs, recycle delays ranging from 20 to 60 s, and 256–2304 transients. The ¹⁹F/¹³C Hartmann-Hahn conditions were calibrated on a poly(tetrafluoroethylene) sample. For all samples containing protons a two-pulse phase modulation (TPPM) decoupling scheme was used with frequency field of 62 kHz, while in the case of samples containing fluorine atoms a swept-frequency two-pulse phase modulation (SW$_f$-TPPM) decoupling scheme[60] was used, with frequency field of 74 kHz. ¹³C and ¹⁵N chemical shift scales were referenced to glycine (¹³C methylene signal at 43.5 ppm) and to $(NH_4)_2SO_4$ (¹⁵N ammonium signal at δ = 24.7 ppm with respect to NH_3), respectively as external standards. All NMR data were processed with Bruker TOPSPIN 2.1 software.
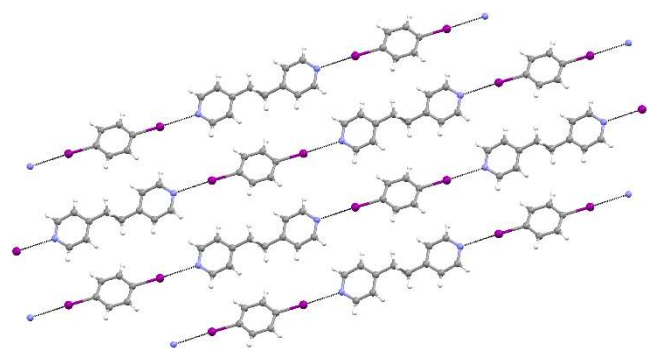
Figure 2. Supramolecular infinite 1D chains in the crystal structure of **3B** viewed along the *b* crystallographic axis. Colour legend: C, grey; H, white; N, light blue; I, magenta.

RESULTS AND DISCUSSION

Thermal and structural characterization of halogen-bonded adducts. Thermal analysis by DSC confirmed the formation of new chemical species by comparing melting points and degradation temperatures of systems obtained on mixing starting materials with melting points of starting materials or of adducts already reported in literature. **2A**, **3A**, **5A**, **6A**, **2B**, **4B**, **5B**, and **6B** pack in the P−1 triclinic space group, **3B** and **4A** crystallize in the monoclinic crystal system in P2₁/n and P2₁/c space groups, respectively, see crystallographic Table S2 in the SI. All the X-bonded systems under study were chosen due to their similar 1D su-

pramolecular arrangement and hence their comparable geometry. All the chosen XB-acceptors and donors are ditopic and both their coordination sites are involved in forming halogen-bonded infinite supramolecular 1D chains, as shown in Figure 2. In all of the obtained structures, XBs tend to be close to linearity: C–X···N (X = Br, I) angles fall, in fact, in the range 172.3–177.5°, see Table 2. The X···N distances are expressed as normalized contacts (R_{XB}) calculated as the ratio $D_{XN} /(r_X + r_N)$, where D_{XN} is the experimental distance between the halogen atoms (X) and the XB-acceptor nitrogen and r_X and r_N are the corresponding vdW radii. The use of R_{XB} allows contacts of chemically different interacting sites to be directly compared.[61] As expected, the shortest, namely the strongest, interactions are those involving iodoperfluorinated XB donors, thanks to the electron-withdrawing effect of the perfluorinated residue, which increases the magnitude of the positive σ-hole on iodine.[7] Except for co-crystals **2A** and **2B**, in all other supramolecular adducts the R_{XB} is shorter for the systems involving **1B** as XB acceptor, due to the higher Lewis base character of **1B** compared to **1A**. Before NMR analysis the composition of the bulk crystalline materials was confirmed by comparing experimental and calculated PXRD patterns, as shown in detail in the SI.

Table 2. Normalized XB contacts (R_{XB}) and C−X···N (X= Br, I) angles ($\theta_{C-X···N}$) for the supramolecular adducts under study.

Co-crystal	R_{XB}	$\theta_{C–X···N}$ (°)
2A	0.85*	177.21 (4)*
	0.88*	176.40 (4)*
3A	0.86	176.1 (1)
4A	0.81	177.3 (1)
5A	0.81	176.7 (2)
6A	0.80	177.5 (6)
2B	0.89	172.3 (3)
3B	0.84	177.41 (6)
4B	0.79	175.8 (3)
5B	0.78	176.3 (1)
6B	0.78	176.97 (6)

*two crystallographically independent X-bonds.

Solid-State NMR Spectroscopy: correlation of NMR data with the strength of XB. *¹⁵N NMR.* The ¹⁵N CPMAS NMR spectra of compounds **2A**–**6A**, **2B**–**6B** and of the starting materials, **1A**, **1B**, are shown in Figure 3 (X-bonded nitrogen region). With the only exception of compound **2A**, in both series it can be noted the occurrence of a systematic low-frequency shift in the signal of the dipyridyl nitrogen upon co-crystal formation, which is consistent with the lone pair sharing for pyridine-like nitrogen atoms.[62] The magnitude of the shift increases going from haloarenes to haloalkanes, and this result is consistent

with the measured distance of the XB, that is, R_{XB}. Specifically, the strongest N···I attraction occurs in **6B**, for which we observed a shift upon XB formation ($\Delta\delta_{iso}$ ^{15}N)
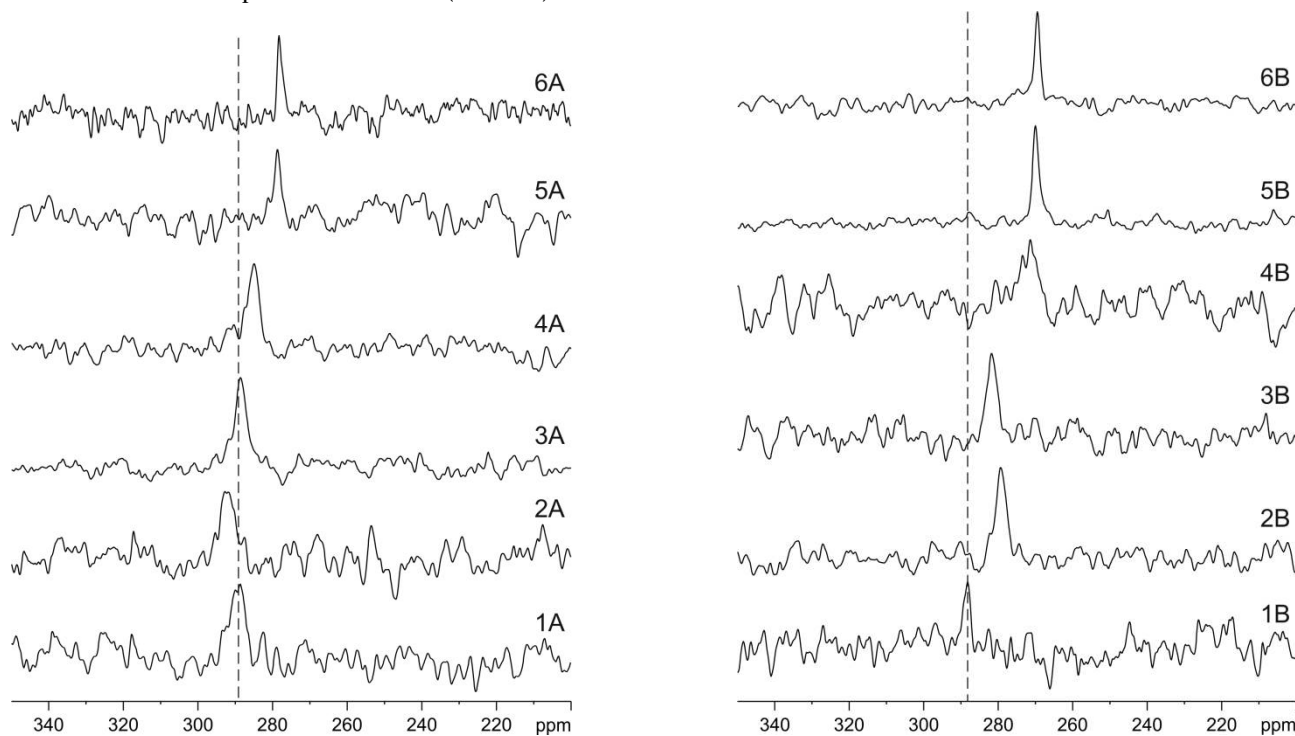
Figure 3. ^{15}N (40.56 MHz) CPMAS spectra of the two series of X-bonded compounds **2A–6A** and **2B–6B**, together with starting materials **1A** and **1B**, recorded at 9 kHz. The vertical lines highlight the systematic shift upon XB formation.

Table 3. Experimental ^{15}N isotropic chemical shift of dipyridyl nitrogens directly involved in XB.

	Comp/co-cryst[a]	δ_{iso} ^{15}N (ppm)[b]	$\Delta\delta_{iso}$ ^{15}N (ppm)[c]		Comp/co-cryst[a]	δ_{iso} ^{15}N (ppm)[b]	$\Delta\delta_{iso}$ ^{15}N (ppm)[c]
1A	Bipy	289.3		**1B**	Bipyet	288.2	
2A	(bipy)·(DBrTFB)	292.2	–3.0	**2B**	(bipyet)·(DBrTFB)	279.3	8.9
3A	(bipy)·(DIB)	288.7	0.6	**3B**	(bipyet)·(DIB)	281.7	6.4
4A	(bipy)·(DITFB)	285.0	4.3	**4B**	(bipyet)·(DITFB)	271.4	15.8
5A	(bipy)·(DIHFO)	278.7	10.5	**5B**	(bipyet)·(DIHFO)	270.0	18.2
6A	(bipy)·(DIDFH)	278.3	11.0	**6B**	(bipyet)·(DIDFH)	269.4	18.8

[a]X-bonded co-crystals are listed top-down in order of increasing XB strength, that is, R_{XB}. [c]Experimental change of the ^{15}N chemical shift upon XB formation, with respect to the corresponding dipyridyl derivative (bipy or bipyet).

as high as 19 ppm (see Table 3). The other compounds exhibit progressively lower $\Delta\delta_{iso}$ ^{15}N, affording an overall trend that dictates the strength of the XB donor in the order DIDFH ≥ DIHFO > DITFB > DBrTFB > DIB for bipyet series, while for bipy series the strength of the XB donors follows the order DIDFH ≥ DIHFO > DITFB > DIB > DBrTFB. The donors hierarchy in bipyet series is in agreement with the one proposed by Aakeröy *et al*;[7] however, the trend does not hold in the bipy series because DIB and DIBrTFB are exchanged with each other. We sought to explain such difference in the following ways. (i) Bipyet is a better XB acceptor than bipy, because of the ethyl moiety that increases its basic character. Therefore, in the bipy series the XB is less strong and, in absence of a pronounced

σ-hole as in the case of DIB and DBrTFB, the XB will be even weaker. Hence, we can infer that other crystal packing effects rather than the XB alone may have an influence on the chemical shifts of **2A** and **3A**, thus altering the donors hierarchy. (ii) The unexpected high-frequency shift in **2A** might be one of the reasons that leads DBrTFB to be a worse XB donor than DIB in bipy series, therefore we explored the changes in the tensor components that occur in the presence of the XB. Owing to the very low ^{15}N natural abundance, the ^{15}N chemical shift tensors could not be experimentally obtained, thus they were computed. The results of GIPAW DFT computations are summarized in Table 4. For purposes of comparison, the isotropic chemical shifts from ^{15}N CPMAS spectra recorded in this work are

also given in the table. The experimental δ_{iso} [15]N values are overestimated by the

Table 4. Calculated[a] nitrogen chemical shift tensors[b] for X-bonded co-crystals herein reported.

| Compound	Ω (ppm)	K	δ_{11} (ppm)[c]	δ_{22} (ppm)[c]	δ_{33} (ppm)[c]	δ_{ave} (ppm)[c]	δ_{iso} (ppm)[d]
1A	659	0.38	629	424	−30	341	314
2A[e]	657	0.38	631	428	−26	344	317
	658	0.38	630	427	−28	343	
3A	645	0.36	628	420	−17	343	313
4A	612	0.40	602	419	−10	337	310
5A	572	0.44	569	409	−3	325	303
6A	577	0.43	573	408	−4	325	303
1B	686	0.36	646	426	−40	344	313
2B	621	0.41	598	416	−23	330	304
3B	614	0.42	593	416	−21	329	306
4B	571	0.43	569	407	−2	324	297
5B	534	0.50	534	401	0	311	295
6B	528	0.49	535	401	7	314	294

[a]PW86PBE-XDM calculation. [b]Chemical shift tensor parameters: span, $\Omega \approx \delta_{11} - \delta_{33}$; skew, $\kappa = 3(\delta_{22} - \delta_{iso})/\Omega$; average of the principal components, $\delta_{ave} = (\delta_{11} + \delta_{22} + \delta_{33})/3$, where $\delta_{11} \geq \delta_{22} \geq \delta_{33}$. [c]All chemical shift tensor components are referenced to liquid NH_3 at 300 K. [d]Experimental isotropic chemical shifts taken from Table 3, referenced to liquid NH_3. [e]Two crystallographically independent nitrogen sites.

calculations by several ppm, even with the adoption of the XDM method. However, while it should be noted that the challenges associated with this type of chemical calculations are not trivial at all, the overestimation of the SSNMR chemical shifts has been systematically reported in the case of XB.[37,39,40] Consistent with previous results,[37] we observed a reduction in the tensor span upon XB formation; the decrease is in the order of 10% for the bipy series, and of 20% for the bipyet series. Without any surprise, the principal components of the chemical shift tensor provide a more sensitive information than the isotropic chemical shift. Indeed, the δ_{iso} range for all systems is in the order of 10–20 ppm, while the change in the principal component is much larger, up to 100 ppm. In particular, the component which changes the most is the least shielded component, δ_{11}: it varies within the range of 62 ppm for bipy series, and 112 ppm for bipyet series. The other two components show narrower ranges: the δ_{22} component changes within the range of 20–25 ppm, while the δ_{33} component falls within the range of 27–47 ppm respectively for bipy and bipyet series.

These results are in excellent agreement with those obtained by Facelli in a study of the changes of the ^{15}N chemical shift tensor in pyridine upon hydrogen bonding formation.[63] According to Facelli's work, the least shielded component δ_{11} lies in the direction tangential to the aromatic ring. The middle principal component δ_{22} also lies in the plane of the molecule and along the radial direction, while the most shielded component δ_{33} lies in the direction perpendicular to the aromatic ring (see Figure 4).

The δ_{11} component is dominated by the n-π^* (lone-pair) transition, which is the one with the smallest energy gap.

The δ_{22} component is dominated by σ_{N-C}-π^* transitions. The δ_{33} component is instead dominated by the σ-electronic structure.[64] Furthermore, according to the Ramsey expression of the chemical shift,[65] the paramagnetic term is inversely proportional to the energy gap between the HOMO and LUMO pair of orbitals; hence, following the decreasing trend observed for δ_{11} and δ_{22} values we may speculate that there should be an increase of the energy difference between orbitals upon XB formation.
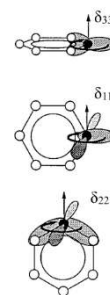

Figure 4. Orientation of the principal components of the ^{15}N chemical shift tensor in pyridine, after Solum et al.[64] The shaded areas represent the electron orbitals making the largest contribution to the chemical shift tensor components.

Such account may be rationalized as follows. Pinter et al. have used accurate DFT calculations to demonstrate that the XB has a non-negligible part of charge transfer character, especially when the halogen and the Lewis base are soft.[66] The same authors pointed out that the observed orbital-interaction stabilization comes from the donation of the lone pair of the halogen acceptor to the σ* orbital of

the donor. For these reasons we think that the orbital-interaction stabilization coming from charge transfer enlarges the gap of the nitrogen n-π^* and σ_{N-C}-π^* transition in the X-bonded compound, thus reducing the δ_{11}, δ_{22} values accordingly. This is true for all the compounds herein but for **2A**, which displays a slight increase of the δ_{11}, δ_{22} components. This opposite behavior helps to explain why the δ_{iso} ^{15}N of the above compound shifts toward high frequency when compared to that of the bipy alone; moreover, the trend is confirmed by the computed δ_{ave} ^{15}N value, which increases with respect to the bipy alone. The accuracy of these accounts should be verified by a thorough DFT study with molecular orbital analysis, including fully relativistic pseudopotentials. However, while the inclusion of relativistic corrections to periodic boundary conditions is still an ongoing area of research,[40] an extensive molecular orbital analysis was beyond the scope of the present work.

^{15}N chemical shifts are a direct source of information about XB surrounding, thus we hypothesized a strong dependence with the XB geometry and strength. This prompted us to examine the experimental correlation between the shift in δ_{iso} ^{15}N upon co-crystal formation and the normalized distance parameter, R_{XB}.
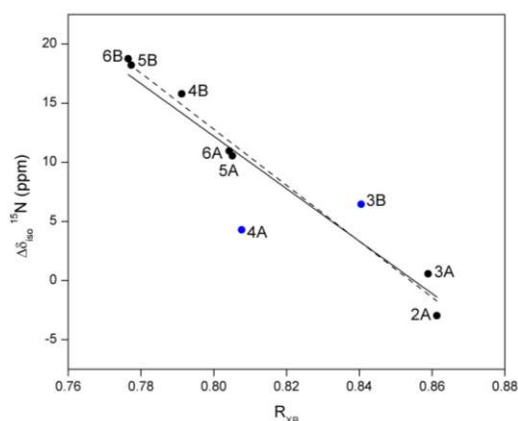
Figure 5. Plot of experimental values of the change in ^{15}N chemical shifts upon co-crystal formation as a function of the corresponding normalized distance parameter. The values are taken from Table 3. The blue circles represent the two X-bonded co-crystals whose space groups are different from the others. The solid line represents the best fit including the latter: $\Delta\delta_{iso}$ ^{15}N = $-221.9R_{XB} + 189.7$, $R^2 = 0.8572$. The dashed line represents the best fit excluding **3B** and **4A** data points: $\Delta\delta_{iso}$ ^{15}N = $-237.0R_{XB} + 202.4$, $R^2 = 0.9798$.

The plot is given in Figure 5; a remarkably good linear correlation is observed ($R^2 = 0.9798$) when the X-bonded co-crystals are taken within the same space group (*i.e.*, P-1). The inclusion of the **3B** and **4A** data points, which crystallize respectively in the P2$_1$/n and P2$_1$/c space groups, dramatically worsen the relationship ($R^2 = 0.8572$). Difficulties lie in comparing such distinct XB geometries, hence such constraints are needed. In addition, we have excluded *a priori* the **2B** datum for two reasons: firstly, because it has

a significantly different angle of interaction (172.3°), probably due to the geometry of the ethyl moiety. Secondly, because it exhibits C–Br bond shortening. The C–X bond shortening upon XB formation is not something unheard of: in fact, Pinter *et al.* have addressed the issue from a molecular orbital perspective.[66] They have attributed the smaller bond length upon XB formation to a modulating effect of the XB acceptor on the orbital energies of X: since the acceptor is electron rich, thus partially negative, the coordination of the acceptor to X elevates the orbital energies of X. Such perturbation results in a smaller energy mismatch between interacting atomic orbitals of C and X, thus making the bond stronger (*i.e.*, shorter). This phenomenon usually takes place upon increasing the hardness of the Lewis base, and this is exactly what happens when we switch from bipy (**2A**) to bipyet (**2B**). The same authors also explain why the C–X bond shortening does not occur with iodine: as previously mentioned, the N···I bond has a non-negligible contribution from charge transfer; however, charge transfer and proximity of negative charge work against each other. Therefore, when the effect of charge transfer is smaller than that of the negative charge, C–X bond shortening happens and *vice versa*. On balance, it can be seen that when the R_{XB} increases, the value of $\Delta\delta_{iso}$ ^{15}N decreases. This is a reasonable trend: as the XB becomes gradually weak, the ^{15}N chemical shifts becomes more similar to that of the starting material. The experimental correlation is reproduced computationally, although the magnitude of the shifts is overestimated (see Figure 6). To the best of our knowledge, this is the first successful correlation between SSNMR ^{15}N chemical shifts and strength of the XB.
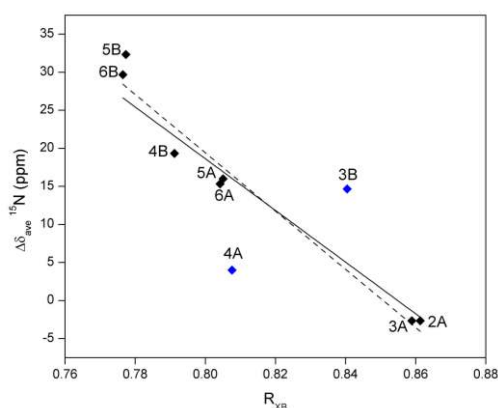
Figure 6. Plot of computed values of the change in chemical shifts upon XB formation as a function of the corresponding normalized distance parameter. The values are taken from Table 4. The blue diamonds represent the two X-bonded compounds whose space groups are different from the others. The solid line represents the best fit including the latter: $\Delta\delta_{ave}$ ^{15}N = $-339.7R_{XB} + 290.4$, $R^2 = 0.7327$. The dashed line represents the best fit excluding **3B** and **4A** data points: $\Delta\delta_{ave}$ ^{15}N = $-382.8R_{XB} + 325.7$, $R^2 = 0.9568$.

13C NMR. Figure 7 presents the covalently bonded C–X regions of the ^{13}C NQS NMR spectra for compounds **2A**–
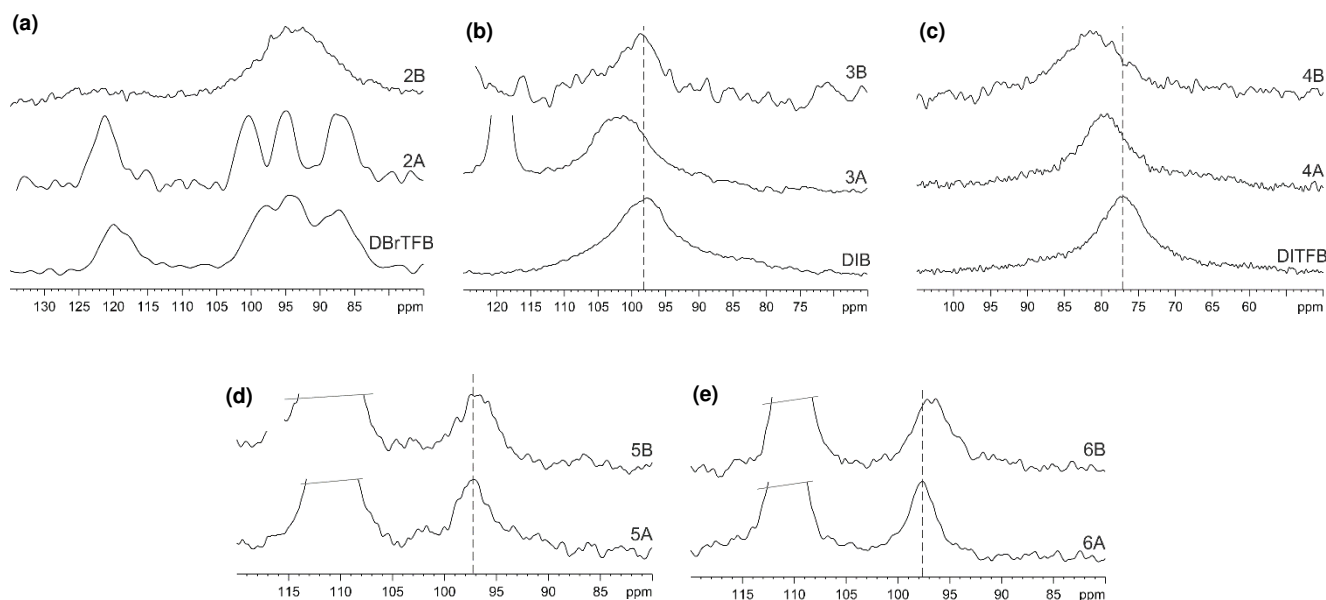
Figure 7. Selected regions corresponding to the C–X resonance of the experimental ^{13}C NQS spectra of X-bonded co-crystals recorded at 12 kHz. The vertical lines highlight the systematic high-frequency shift upon XB formation in (b) and (c). The starting materials do not appear in (d) and (e) because they melted inside the rotor.

6A, **2B**–**6B**. Analogous spectra of the pure starting material are also shown. In order to get sensitivity enhancement, when possible we performed a NQS experiments with ^{19}F/^{13}C CP instead of the standard ^{1}H/^{13}C CP, thus improving the signal-to-noise ratio of the C–X signals with a dramatic reduction of the number of scans. The observed isotropic chemical shifts for the carbon nuclei are given in Table 5. The full ^{13}C NQS NMR spectra and chemical shift assignments may be found in the Supporting Information. It is well known[39-42] that the ^{13}C resonances of carbons covalently bonded to quadrupolar nuclei are broadened or even split due to second-order quadrupolar effects *via* residual dipolar coupling (RDC). This phenomenon enlarges the error in ^{13}C isotropic chemical shifts measurement. In general no splitting or asymmetric broadening was observed for the peaks of carbon atoms bonded to iodine, while for the carbons bonded to bromine we observed the characteristic asymmetric quartet[67] arising from second order effects. It was mentioned in the introduction that the ^{13}C SSNMR chemical shift of carbon atoms bonded to iodine in both aromatic[39-41] and C(sp)[12,42] XB donors are known to increase upon XB formation. Consistent with these data, the spectra presented in Figure 7 clearly show an increase of δ_{iso} ^{13}C relative to the pure compounds when XB occurs. The chemical shift of carbon directly bonded to bromine atom also move to higher frequencies upon XB formation although the extent of the shift is quite modest (about 1 ppm) when compared to the carbon-iodine system. For co-crystals **5A**, **6A**, **5B**, and **6B**, the lack of the starting materials spectra prevents us from observing whether the same trend upholds.

Table 5. ^{13}C Isotropic chemical shifts of carbons covalently bonded to halogen atoms.

	Comp/co-cryst	δ_{iso} ^{13}C (ppm)	d_{C-X} (Å)
	DBrTFB	99.9	1.867
	DITFB	77.0	2.075
	DIB	98.2	2.091
	DIDFH	n/a[a]	n/a[b]
	DIHFO	n/a[a]	n/a[b]
2A	[(bipy)(DBrTFB)]	100.9[c]	n/a[c]
3A	[(bipy)(DIB)]	101.7	2.105
4A	[(bipy)(DITFB)]	79.6	2.094
5A	[(bipy)(DIHFO)]	97.1	2.162
6A	[(bipy)(DIDFH)]	97.6	2.149
2B	[(bipyet)(DBrTFB)]	95.9[d]	1.860
3B	[(bipyet)(DIB)]	99.8	2.112
4B	[(bipyet)(DITFB)]	81.2	2.101
5B	[(bipyet)(DIHFO)]	96.7	2.149
6B	[(bipyet)(DIDFH)]	96.8	2.157

[a]Not applicable due to low melting temperatures (powder melts inside the rotor). [b]Lack of SCXRD data. [c]Two resonances for two carbon sites were expected in **2A**. [d]Estimated value due to the presence of unresolved quadruplet.
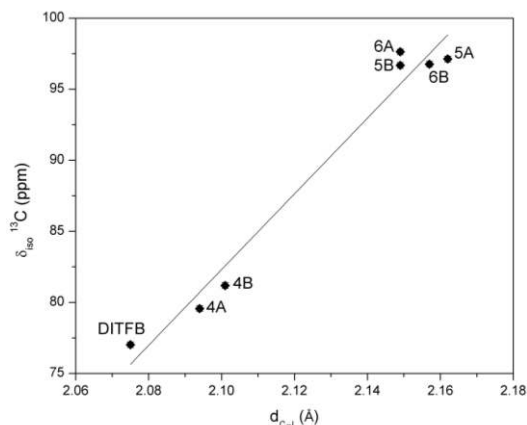
Figure 8. Plot of the experimental values of ^{13}C chemical shift of carbons covalently bonded to iodine. The values are taken from Table 5. The best fit is represented by a linear function: δ_{iso} $^{13}C = 266.5d_{C-I} - 477.3$, $R^2 = 0.9664$.

As for nitrogen chemical shift, we tried to correlate the ^{13}C chemical shifts to the changes of the XB environment by plotting δ_{iso} ^{13}C values as a function of the corresponding C–I distances, d_{C-I} (see Figure 8). We observed a reasonable trend with a remarkable linear correlation ($R^2 = 0.9664$), even considering the pure DITFE. This is consistent with the computed linear fit between δ_{iso} ^{13}C values and their respective C–I distances reported by Bryce and collaborators.[40] The trend is also in nice agreement with ^{15}N data related to the strength of the different XB donors: stronger XBs are associated with higher shift values. It is worthy to note that this trend comprises both aromatic and aliphatic sp[3] carbons, thus giving a better overview of the ^{13}C SSNMR chemical shifts of X-bonded compounds, as well as linking the sparse data already present in the literature.

CONCLUSIONS

The present contribution demonstrates the ability of SSNMR spectroscopy to directly investigate the XB with a simple technique such as CPMAS avoiding the challenging examination of halogen atoms, which are affected by well-known issues, such as excessive line-broadening, extremely expensive hardware, and complicated pulse sequences. The problem has been tackled by selecting prototypical 1D X-bonded co-crystals[61] exhibiting various types of C–X···N (X = I, Br) interactions. These co-crystals have been separated in two series based upon two different XB acceptors, arranging them in rank order on the basis of their normalized distance parameter, R_{XB}, which is a convenient indicator of the interaction strength. By doing so, we wanted to verify whether this crystallographic trend could be reproduced by means of ^{15}N and ^{13}C SSNMR, thus giving us the chance to test the ability of the technique in quantifying the XB strength.

For both series, the solid-state ^{15}N chemical shifts generally decrease upon XB formation. When the change of chemical shifts is plotted against the corresponding R_{XB} value, a good linear correlation is observed. This experimental

trend has been reproduced reasonably well by GIPAW DFT calculations. Indeed an interesting relationship between solid-state ^{15}N chemical shifts and the strength of the XB has been successfully determined.

For co-crystals **2A–4A** and **2B–4B**, the solid-state ^{13}C chemical shifts generally increase upon XB formation. This trend could not be examined for co-crystals **5A, 6A**, and **5B, 6B**, owing to the solid-liquid phase transition of the starting materials inside the magnet. Nonetheless, we were able to establish a correlation between the isotropic value of the carbon chemical shifts and the C–I distance: as the chemical shift increases, so does the C–I length. This correlation has demonstrated to be reliable only within comparable C–X environments, *i.e.*, within iodoperfluorobenzene or bromoperfluorobenzene series. Indeed, correlations with the R_{XB} have not been observed experimentally, perhaps due do the many different carbon environments considered.

Overall, this work provides an effective method for the direct detection of the XB by natural abundance ^{15}N SSNMR. The ^{15}N isotropic chemical shifts are diagnostic of the strength of the XB, and demonstrated to be more sensitive probes of the XB than ^{13}C chemical shifts in a large set of X-bonded systems. Further studies on different XB motifs may extend the use of SSNMR as a first-choice technique when preliminary characterization of XB compounds is required.

ASSOCIATED CONTENT

Supporting Information. Additional experimental and computational details, full ^{13}C SSNMR spectra and assignments, crystallographic data for **3B**, **5B**, and **6B**, powder X-ray diffractograms, thermal and FTIR analyses, and calculated NMR tensors. This material is available free of charge via the Internet at http://pubs.acs.org.

AUTHOR INFORMATION

Corresponding Authors

*(R.G.) E-mail: roberto.gobetto@unito.it. Tel: +390116707520
*(P.M.) E-mail: pierangelo.metrangolo@polimi.it. Tel: +390223993041

REFERENCES

(1) (a) Metrangolo, P; Resnati, G.; Pilati, T.; Biella, S. *Halogen Bonding: Fundamentals and Applications;* Springer: Berlin, **2008**; Structure and Bonding Vol. 126, pp 105-136. (b) Metrangolo, P.; Meyer, F.; Pilati, T.; Resnati, G.; Terraneo, G. *Angew. Chem., Int. Ed.* **2008**, *47*, 6114-6127. (c) Mukherjee, A.; Tothadi, S.; Desiraju G. R. *Acc. Chem Res.* **2014**, *47*, 2514-2524.

(2) (a) Priimagi, A.; Cavallo, G.; Metrangolo, P.; Resnati, G. *Acc. Chem. Res.* **2013**, *46*, 2886-2895. (b) Meyer, F.; Dubois, P. *CrystEngComm* **2013**, *15*, 3058-3071.

(3) (a) Voth, A. R.; Khuu, P.; Oishi, K.; Ho, P. S. *Nat. Chem.* **2009**, 1, 74-79. (b) Metrangolo, P.; Resnati, G. *Nat. Chem.* **2012**, *4*, 437-438. A. Bertolani, L. Pirrie, L. Stefan, N. Houbenov, J. S. Haataja, L. Catalano, G. Terraneo, G. Giancane, L. Valli, R. Milani, O. Ikkala, G. Resnati and P. Metrangolo, *Nat. Commun.*, **2015**, **6**, 7574.

(4) Corradi, E.; Meille, S. V.; Messina, M. T.; Metrangolo, P.; Resnati G. *Angew. Chem., Int. Ed.* **2000**, *39*, 1782-1786.

(5) Metrangolo, P.; Resnati, G. *Chem. Eur. J.* **2001**, 7, 2511-2519.

(6) Metrangolo, P.; Neukirch, H.; Pilati, T.; Resnati, G. *Acc. Chem. Res.* **2005**, *38*, 386-395.

(7) Aakeröy, C. B., M.; Desper, J.; Metrangolo, P.; Resnati, G. *Chem. Eur. J.* **2013**, *19*, 16240-16247.

(8) Lommerse, J. P. M.; Stone, A. J.; Taylor, R.; Allen, F. H. *J. Am. Chem. Soc.* **1996**, *118*, 3108-3116.

(9) Walsh, R.; Padgett, C. W.; Metrangolo, P.; Resnati, G.; Hanks, T. W.; Pennington, W. T. *Cryst. Growth Des.* **2001**, *1*, 165-175.

(10) (a) Luo, L.; Wilhelm, C.; Sun, A.; Grey, C. P.; Lauher, J. W.; Goroff, N. S. *J. Am. Chem. Soc.* **2008**, *130*, 7702-7709. (b) Houbenov, N.; Milani, R.; Puotanen, M.; Haataja, J.; Dichiarante, V.; Sainio, J.; Ruokolainen, J.; Resnati, G.; Metrangolo, P.; Ikkala, O. *Nat. Commun.* **2014**, 5, 4043.

(11) (a) Wuest, J. D. *Nat. Chem.* **2012**, *4*, 74-75. (b) Priimagi, A.; Cavallo, G.; Forni, A.; Gorynsztejn-Leben, M.; Kaivola, M.; Metrangolo, P.; Milano, R.; Shishido, A.; Pilati, T.; Resnati, G.; Terraneo, G. *Adv. Funct. Mater.* **2012**, 22, 2572-2579.

(12) Baldrighi, M.; Cavallo, G.; Chierotti, M. R.; Gobetto, R.; Metrangolo, P.; Pilati, T.; Resnati, G.; Terraneo, G. *Mol. Pharmaceutics* **2013**, *10*, 1760-1772.

(13) Martí-Rujas, J.; Colombo, L.; Lü, J.; Dey, A.; Terraneo, G.; Metrangolo P.; Pilati, T.; Resnati, G. *ChemComm* **2012**, *48*, 8207-8209.

(14) Metrangolo, P.; Carcenac, Y.; Lahtinen, M.; Pilati, T.; Rissanen, K.; Vij, A.; Resnati, G. *Science* **2009**, *323*, 1461-1464.

(15) Cavallo, G.; Metrangolo, P.; Pilati, T.; Resnati, G.; Sansotera, M.; Terraneo, G. *Chem. Soc. Rev.* **2010**, *39*, 3772-3783.

(16) Langton, M. J.; Robinson, S. W.; Marques, I.; Felix, V.; Beer, P. D. *Nat. Chem.* **2014**, *6*, 1039-1043.

(17) Jentzsch, A. V.; Emery, D.; Mareda, J.; Nayak, S. K.; Metrangolo, P.; Resnati, G.; Sakai, N.; Matile, S. *Nat. Commun.* **2012**, *3*, 905.

(18) Desiraju, G. R.; Ho, P. S.; Kloo, L.; Legon, A. C.; Marquardt, R.; Metrangolo, P.; Politzer, P.; Resnati, G.; Rissanen, K. *Pure Appl. Chem.* **2013**, *85*, 1711-1713.

(19) (a) Clark, T; Hennemann, M.; Murray, J. S.; Politzer, P. *J. Mol. Mod.* **2007**,*13*, 291-296. (b) Politzer, P.; Lane, P.; Concha, M. C.; Ma, Y.; Murray, J. S. *J. Mol. Mod.* **2007**, *13*, 305-311.

(20) (a) Larsen, D. W.; Allred, A. L. *J. Phys. Chem.* **1965**, *69*, 2400–2401. (b) Bent, H. A. *Chem. Rev.* **1968**, *68*, 587–648. (c) Dumas, J.-M.; Gomel, M. *J. Chim. Phys.* **1975**, *72*, 953–955. (d) Bailey, R. D.; Drake, G. W.; Grabarczyk, M.; Hanks, T. W.; Hook, L. L.; Pennington, W. T. *J. Chem. Soc., Perkin Trans. 2* **1997**, 2773–2780.

(21) Thorson, R. A.; Woller, G. R.; Driscoll, Z. L.; Geiger, B. E.; Moss, C. A.; Schlapper, A. L.; Speetzen, E. D.; Bosch, E.; Erdelyi, M.; Bowling, N. P. *Eur. J. Org. Chem.* **2015**, 1685–1695.

(22) (a) Messina, M. T.; Metrangolo, P.; Navarrini, W.; Radice, S.; Resnati, G.; Zerbi, G. *J. Mol. Struct.* **2000**, *524*, 87–94. (b) Hauchecorne, D.; Herrebout, W. A. *J. Phys. Chem. A* **2013**, *117*, 11548–11557. (c) Hauchecorne, D.; van der Veken, B. J.; Moiana, A.; Herrebout, W. A. *Chem. Phys.* **2010**, *374*, 30–36.

(23) (a) Legon, A. C. *Angew. Chem., Int. Edit.* **1999**, *38*, 2687–2714. (b) Legon, A. C. *Phys. Chem. Chem. Phys.* **2010**, *12*, 7736–7747.

(24) (a) Murray-Rust, P.; Motherwell, W. D. S. *J. Am. Chem. Soc.* **1979**, *101*, 4374–4376. (b) Mooibroek, T. J.; Gamez, P. *CrystEngComm* **2013**, *15*, 4565–4570.

(25) (a) Politzer, P.; Murray, J. S. *ChemPhysChem* **2013**, *14*, 278–294. (b) Riley, K. E.; Hobza, P. *Phys. Chem. Chem. Phys.* **2013**, *15*, 17742–17751.

(26) Karpfen, A. *Halogen Bonding: Fundamentals and Applications*; Springer: Berlin, **2008**; Structure and Bonding Vol. 126, pp 1–15.

(27) (a) Bertrán, J. F.; Rodríguez, M. *Org. Magn. Reson.* **1979**, *12*, 92–94. (b) Rodríguez, M.; Bertrán, J. F. *Org. Magn. Reson.* **1980**, *14*, 244–246.

(28) (a) Cardillo, P.; Corradi, E.; Lunghi, A.; Valdo Meille, S.; Teresa Messina, M.; Metrangolo, P.; Resnati, G. *Tetrahedron* **2000**, *56*, 5535–5550. (b) Metrangolo, P.; Panzeri, W.; Recupero, F.; Resnati, G. *J. Fluor. Chem.* **2002**, *114*, 27–33. (c) De Santis, A.; Forni, A.; Liantonio, R.; Metrangolo, P.; Pilati, T.; Resnati, G. *Chem. Eur. J.* **2003**, *9*, 3974–3983. (d) Metrangolo, P.; Pilati, T.; Resnati, G.; Stevenazzi, A. *Curr. Opin. Colloid Interface Sci.* **2003**, *8*, 215–222.

(29) (a) Dimitrijević, E.; Kvak, O.; Taylor, M. S. *Chem. Commun.* **2010**, *46*, 9025–9027. (b) Sarwar, M. G.; Dragisic, B.; Salsberg, L. J.; Gouliaras, C.; Taylor, M. S. *J. Am. Chem. Soc.* **2010**, *132*, 1646–1653.

(30) (a) Libri, S.; Jasim, N. A.; Perutz, R. N.; Brammer, L. *J. Am. Chem. Soc.* **2008**, *130*, 7842–7844. (b) Beweries, T.; Brammer, L.; Jasim, N. A.; McGrady, J. E.; Perutz, R. N.; Whitwood, A. C. *J. Am. Chem. Soc.* **2011**, *133*, 14338–14348.

(31) Rege, P. D.; Malkina, O. L.; Goroff, N. S. *J. Am. Chem. Soc.* **2002**, *124*, 370–371.

(32) Castro-Fernández, S.; Lahoz, I. R.; Llamas-Saiz, A. L.; Alonso-Gómez, J. L.; Cid, M.-M.; Navarro-Vázquez, A. *Org. Lett.* **2014**, *16*, 1136–1139.

(33) (a) Carlsson, A.-C. C.; Gräfenstein, J.; Budnjo, A.; Laurila, J. L.; Bergquist, J.; Karim, A.; Kleinmaier, R.; Brath, U.; Erdélyi, M. *J. Am. Chem. Soc.* **2012**, *134*, 5706–5715. (b) Hakkert, S. B.; Erdélyi, M. *J. Phys. Org. Chem.* **2015**, *28*, 226–233.

(34) Blackstock, S. C.; Lorand, J. P.; Kochi, J. K. *J. Org. Chem.* **1987**, *52*, 1451–1460.

(35) Bouchmella, K.; Dutremez, S. G.; Alonso, B.; Mauri, F.; Gervais, C. *Cryst. Growth Des.* **2008**, *8*, 3941–3950.

(36) Weingarth, M.; Raouafi, N.; Jouvelet, B.; Duma, L.; Bodenhausen, G.; Boujlel, K.; Schöllhorn, B.; Tekely, P. *Chem. Commun.* **2008**, 5981–5983.

(37) Viger-Gravel, J.; Korobkov, I.; Bryce, D. L. *Cryst. Growth Des.* **2011**, *11*, 4984–4995.

(38) Attrell, R. J.; Widdifield, C. M.; Korobkov, I.; Bryce, D. L. *Cryst. Growth Des.* **2012**, *12*, 1641–1653.

(39) Widdifield, C. M.; Cavallo, G.; Facey, G. A.; Pilati, T.; Lin, J.; Metrangolo, P.; Resnati, G.; Bryce, D. L. *Chem. Eur. J.* **2013**, *19*, 11949–11962.

(40) Viger-Gravel, J.; Leclerc, S.; Korobkov, I.; Bryce, D. L. *CrystEngComm* **2013**, *15*, 3168–3177.

(41) Viger-Gravel, J.; Leclerc, S.; Korobkov, I.; Bryce, D. L. *J. Am. Chem. Soc.* **2014**, *136*, 6929–6942.

(42) Baldrighi, M.; Bartesaghi, D.; Cavallo, G.; Chierotti, M. R.; Gobetto, R.; Metrangolo, P.; Pilati, T.; Resnati, G.; Terraneo, G. *CrystEngComm* **2014**, *16*, 5897–5904.

(43) Nonappa; Lahtinen, M.; Kolehmainen, E.; Haarala, J.; Shevchenko, A. *Cryst. Growth Des.* **2013**, *13*, 346–351.

(44) Viger-Gravel, J.; Meyer, J. E.; Korobkov, I.; Bryce, D. L. *CrystEngComm* **2014**, *16*, 7285–7297.

(45) (a) Bailey, R. D.; Drake, G. W.; Grabarczyk, M.; Hanks, T.W.; Hook, L. L.; Pennington, W. T., *J. Chem. Soc. Perkin Trans. 2*, 1997, 2773–2780; (b) Messina, M. T.; Metrangolo, P.; Panzeri, W.; Pilati, T.; Resnati, G. *Tetrahedron*, **2001**, *57*, 8543–8570; (c) Corradi, E.; Meille, S. V.; Messina, M. T.; Metrangolo, P.; Resnati, G. *Tetrahedron Lett.***1999**, *40*, 7519–7523; (d) Walsh, R. B.; Padgett,

C. W.; Metrangolo, P.; Resnati, G.; Hanks, T. W.; Pennington, W. T. *Cryst. Growth Des.* **2001**, *1*, 20, 165–175.

(46) Sheldrick, G. M. *Acta Crystallogr. Sect. A* **2008**, *64*, 112–122.

(47) Macrae, C. F.; Bruno, I. J.; Chisholm, P. R.; Edgington, P. R.; McCabe, P; Pidcock, E.; Rodriguez-Monge, L.; Taylor, R.; van de Streek, J.; Wood, P. A. *J. Appl. Cryst.* **2008**, *41*, 466–470.

(48) Spek, A. L. *Acta Crystallogr. Sect. D* **2009**, *65*, 148–155.

(49) Giannozzi, P.; Baroni, S.; Bonini, N.; Calandra, M.; Car, R.; Cavazzoni, C.; Ceresoli, D.; Chiarotti, G. L.; Cococcioni, M.; Dabo, I.; Dal Corso, A.; de Gironcoli, S.; Fabris, S.; Fratesi, G.; Gebauer, R.; Gerstmann, U.; Gougoussis, C.; Kokalj, A.; Lazzeri, M.; Martin-Samos, L.; Marzari, N.; Mauri, F.; Mazzarello, R.; Paolini, S.; Pasquarello, A.; Paulatto, L.; Sbraccia, C.; Scandolo, S.; Sclauzero, G.; Seitsonen, A. P.; Smogunov, A.; Umari, P.; Wentzcovitch, R. M. *J. Phys.: Condens. Matter* **2009**, *21*, 395502.

(50) Perdew, J.; Burke, K.; Ernzerhof, M. *Phys. Rev. Lett.* **1996**, *77*, 3865–3868.

(51) Perdew, J. P.; Wang, Y. *Phys. Rev. B* **1986**, *33*, 8800.

(52) (a) Otero-de-la Roza, A.; Johnson, E. R. *J. Chem. Phys.* **2013**, *138*, 204109; (b) Otero-de-la Roza, A.; Johnson, E. R.; DiLabio, G. A. *J. Chem. Theory Comput.* **2014**, *10*, 5436–5447.

(53) Kresse, G.; Joubert, D. *Phys. Rev. B* **1999**, *59*, 1758–1775.

(54) Pickard, C. J.; Mauri, F. *Phys. Rev. B* **2001**, *63*, 245101.

(55) Jameson, C. J.; Jameson, A. K.; Oppusunggu, D.; Wille, S.; Burrell, P. M.; Mason, J. *J. Chem. Phys.* **1981**, *74*, 81–88.

(56) Monkhorst, H. J.; Pack, J. D. *Phys. Rev. B* **1976**, *13*, 5188–5192.

(57) Franco, F.; Baricco, M.; Chierotti, M. R.; Gobetto, R.; Nervi, C. *J. Phys. Chem. C* **2013**, *117*, 9991–9998.

(58) Metz, G.; Wu, X.; Smith, S. *J. Magn. Reson. Ser. A* **1994**, *110*, 219–227.

(59) Bennett, A.; Rienstra, C.; Auger, M.; Lakshmi, K.; Griffin, R. *J. Chem. Phys.* **1995**, *103*, 6951–6958.

(60) Thakur, R. S.; Kurur, N. D.; Madhu, P. K. *Chem. Phys. Lett.* **2006**, *426*, 459–463.

(61) Cavallo, G.; Metrangolo, P.; Milani, R.; Pilati, T.; Priimagi, A.; Resnati, G.; Terraneo, G. *Chem. Rev.* **2016**, *116*, 2478-2601.

(62) Levy, G. C.; Lichter, R. L. *Nitrogen-15 Nuclear Magnetic Resonance Spectroscopy*; John Wiley & Sons: New York, 1979.

(63) Facelli, J. C. *Chem. Phys. Lett.* **2000**, *322*, 91–96.

(64) Solum, M. S.; Altmann, K. L.; Strohmeier, M.; Berges, D. A.; Zhang, Y.; Facelli, J. C.; Pugmire, R. J.; Grant, D. M. *J. Am. Chem. Soc.* **1997**, *119*, 9804–9809.

(65) Ramsey, N. F. *Phys. Rev.* **1950**, *78*, 699–703.

(66) Pinter, B.; Nagels, N.; Herrebout, W. A.; De Proft, F. *Chem. Eur. J.* **2013**, *19*, 519–530.

(67) Aliev, A.; Harris, K.; Harris, R.; Carss, S.; Olivieri, A. *J. Chem. Soc.-Faraday Trans.* **1995**, *91*, 3167–3176.

TOC